# Sheared force networks: Anisotropies, yielding, and geometry

Snoeijer, J.H.; Ellenbroek, W.G.; Vlugt, T.J.H.; Hecke, M.L. van

# Sheared Force Networks: Anisotropies, Yielding, and Geometry

Jacco H. Snoeijer,[1] Wouter G. Ellenbroek,[2] Thijs J. H. Vlugt,[3] and Martin van Hecke[4]

[1]*Physique et Mécanique des Milieux Hétérogènes, UMR 7636 CNRS-ESPCI, 10 rue Vauquelin, 75231 Paris Cedex 05, France*

[2]*Instituut-Lorentz, Universiteit Leiden, Postbus 9506, 2300 RA Leiden, The Netherlands*

[3]*Condensed Matter and Interfaces, Utrecht University, P.O. Box 80.000, 3508 TA Utrecht, The Netherlands*

[4]*Kamerlingh Onnes Lab, Leiden University, PO box 9504, 2300 RA Leiden, The Netherlands*

(Received 17 August 2005; published 9 March 2006)

A scenario for the yielding of granular matter is presented by considering the ensemble of force networks for a given contact network and applied shear stress $\tau$. As $\tau$ is increased, the probability distribution of contact forces becomes highly anisotropic, the difference between average contact forces along minor and major axes grows, and the allowed networks span a shrinking subspace of all force networks. Eventually, contacts start to break, and at the maximal shear stress the packing becomes effectively isostatic. The size of the allowed subspace exhibits simple scaling properties, which lead to a prediction for the yield stress for packings of an arbitrary contact number.

DOI: 10.1103/PhysRevLett.96.098001 PACS numbers: 45.70.Cc, 05.40.−a, 46.65.+g

Granular media, foams, and emulsions are amorphous materials that can jam and then sustain a certain amount of shear stress before yielding [1–5]. If one slowly increases the applied shear stress and follows the evolution of contact forces and grain locations for such systems, one encounters a rather complex set of phenomena. First, before the system yields as a whole, there are nonadiabatic precursor events such as local rearrangements and microslip [6–8]. Second, the interparticle contact forces in these systems are organized into highly anisotropic and fragile force networks [9–13]—see Fig. 1. Unraveling these shear-induced phenomena and their impact on macroscopic unjamming has remained a great challenge.

While the contact forces evolve to satisfy the applied stresses, the selection of a *specific* force network for a single numerical experiment hinges on microscopic details and packing history. On the other hand, features like contact force probabilities have turned out to be relatively insensitive to these subtle details [11–15], which suggest the use of a purely statistical approach. In this Letter we characterize granular packs under shear stress by studying *ensembles* of force networks for fixed contact networks [16–21]. This approach is based on the fact that in jammed systems there are more contact forces than force balance equations—the ensemble simply consists of all those force networks for which the contact forces are repulsive, balance on every grain, and satisfy global stress constraints, while keeping the geometry fixed. This provides a novel access to the statistics of force networks under shear stress, in which the roles of fabric and force anisotropy are separated explicitly.

We consider ensembles of sheared force networks for frictionless disks in two dimensions, for contact numbers $z$ ranging from the lower limit $z \approx z_c = 4$ (isostatic [22]) to $z = 6$ (strongly hyperstatic). We recover a number of experimental features, in particular, a transition to yielding. We show that force networks, in which purely repulsive forces satisfy force balance on every grain while also sustaining the applied shear stress, cease to exist beyond a critical stress $\tau_m$. This maximum stress $\tau_m$, which is an upper bound for the yield stress $\tau_y$, strongly depends on the coordination number [Fig. 1(a)].

*Force ensemble.*—The numerical results have been obtained by a recently developed ensemble technique [17–21]. The input of the ensemble consists of a fixed contact geometry of a 2D packing of $N = 1024$ frictionless disks of radii $R_i$ with centers $\mathbf{r}_i$ and coordination number $z > z_c$ in a volume $V$, which we generated from molecular dynamics simulations of a 50:50 binary mixture of particles with size ratio 1.4 that have a purely repulsive Lennard-Jones interaction; results presented in this Letter are independent of the potential. Different densities were used to obtain different $z$, typical deformations ranging from 1% to get $z = 4.3$ to about 30% for $z = 6$. The system is *not*

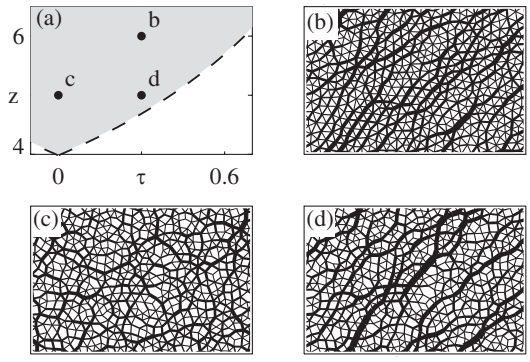


FIG. 1. (a) Overview of the $z$-$\tau$ parameter space, where $z$ and $\tau$ denote coordination number and shear stress, respectively. For a given $z$, force networks cease to exist beyond a maximum $\tau_m$ [dashed line, Eq. (8)]. The dots indicate the values of $\tau$ and $z$ in (b)–(d). (b)–(d) Parts of the force networks, where line thicknesses represent the strength of the contact forces. These networks become highly anisotropic under shear stress.

 

sheared, and the resulting contact networks are isotropic [2,17]. These *contact* networks are then kept fixed, and the positive interparticle forces between particles $i$ and $j$, $f_{ij} \equiv |\mathbf{f}_{ij}|$, are seen as degrees of freedom that satisfy mechanical equilibrium, restricted by the macroscopic stress $\sigma_{\alpha\beta}$:

$$\sum_j f_{ij} \frac{\mathbf{r}_i - \mathbf{r}_j}{|\mathbf{r}_i - \mathbf{r}_j|} = \mathbf{0}, \qquad \sigma_{\alpha\beta} = \frac{1}{V} \sum_{\{ij\}} (\mathbf{f}_{ij})_\alpha (\mathbf{r}_i - \mathbf{r}_j)_\beta. \tag{1}$$

In this picture there are $(zN/2)$ degrees of freedom (contact forces) constrained by $(2N + 3)$ equations, leading, for $z > 4$, to an *ensemble of force networks* that forms a high-dimensional convex subspace $\mathbf{F}_\tau$ [17–19]. The actual ensemble calculation amounts to sampling this force space using a simulated annealing procedure, described in detail in Ref. [18], where it was shown that it samples the force space uniformly. Because of the fixed contact geometry, all resulting networks have an isotropic fabric. The forces, however, become more and more anisotropic as a higher shear stress is imposed on the ensemble. In this Letter we choose the coordinates and pressure such that $\sigma_{xx} = \sigma_{yy} = 1/2$, and consider the dimensionless shear stress $\tau = \sigma_{xy}/\sigma_{xx}$ (equivalent to the relative deviatoric stress) [see Fig. 2(a)].

*Angle resolved force distributions.*—To characterize the anisotropic force networks, we introduce here the contact-angle resolved force distribution $P_\phi(f)$. This is a natural extension of the overall force distribution $P(f)$ [11–15] and acts as a sensitive probe for anisotropy due to shear. Figure 2(b) illustrates that for sheared systems $P_\phi(f)$ modulates with $\phi$—this modulation has its extrema along major and minor axes. Many contact forces along the minor axis ($\phi \sim 3\pi/4$) evolve towards zero for increasing shear, effectively breaking these contacts [17] and leading to a $\delta$ peak at $f = 0$ [black area in Fig. 2(b4)]. These angle resolved distributions allow a straightforward interpretation of the observed broadening or disappearance of the peak of $P(f)$ [1,2,13–15]. Moreover, they can act as a sensitive tool for the comparison of force data from experiments, numerics, and theory [13].

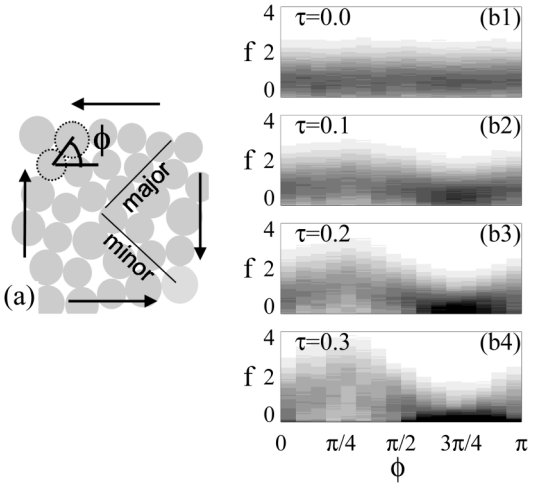


FIG. 2. (a) Illustration of our geometry, showing the direction of shear stress (arrows), contact angle $\phi$, and major and minor axes. (b) Angle resolved force distributions for $z = 5$. $P_\phi(f)$ becomes increasingly modulated with contact angle $\phi$ for increasing shear stress $\tau$.

*Analytical bounds on $\tau$.*—The most basic manifestation of stress anisotropy, however, is the modulation of the average force, $\bar{f}(\phi)$, as a function of the contact orientation. This effect is clearly visible in Fig. 1 and has only recently been accessed experimentally [10,13]. In Fig. 3 we therefore show examples of $\bar{f}(\phi)$ for various stresses and contact numbers, as obtained by the ensemble. For the strongly hyperstatic case [Figs. 3(b) and 3(d)], it is clear that the anisotropy is limited by the requirement that $\bar{f}(\phi)$ should definitely remain positive for all $\phi$. This is due to the repulsive nature of the contact forces, which requires all $f_{ij} \geq 0$.

This simple criterion imposes an analytical bound on the maximum shear stress $\tau_m$ that becomes increasingly accurate for strongly hyperstatic packings. This bound can be computed from the probabilistic version of Eq. (1), which for isotropic contacts reads

$$\sigma_{\alpha\beta} = \frac{\bar{r} N_c}{V\pi} \int_0^\pi d\phi \bar{f}(\phi) n_\alpha n_\beta, \tag{2}$$

where $\bar{r}$ is the average particle radius [23], while $(n_x, n_y) = (\cos\phi, \sin\phi)$; in the remainder we set the prefactor $\bar{r}N_c/V$ equal to unity. We Fourier expand $\bar{f}(\phi)$ as $\sum a_k \sin 2k\phi + \sum b_k \cos 2k\phi$, and anticipate that only odd $k$ sine terms and even $k$ cosine terms are compatible with the symmetry of a simple shear [3]. Equation (2) then yields

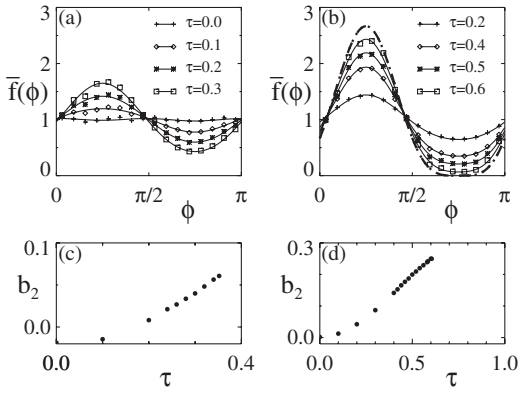


FIG. 3. Average contact force as a function of contact angle $\phi$ and applied shear stress $\tau$. (a) $\bar{f}(\phi)$, for $z = 5$ develops a sinusoidal modulation when $\tau$ is increased. $\bar{f}(\phi)$ can be fitted well by an expression of the form $1 + 2\tau \sin 2\phi - b_2 \cos 4\phi$; $b_2$ slowly increases with $\tau$ as shown in (c). (b) $\bar{f}(\phi)$, for $z = 6$ develops a strong second harmonic for large $\tau$ and approaches the limiting curve given by Eq. (4) (dashed curve). (c),(d) Corresponding dependence of $b_2$ on $\tau$.

$$\bar{f}(\phi) = 1 + 2\tau \sin 2\phi - b_2 \cos 4\phi + \cdots, \quad (3)$$

where the coefficients of the higher order terms $b_2, \ldots$, are independent of the stress tensor (Fourier modes with $k \geq 2$ yield zero upon integration). The role of the higher order terms is limited [24]: our numerics show a significant contribution to $\bar{f}(\phi)$ for large $\tau$ and $z$ for $k = 2$ only [Figs. 3(b) and 3(d)]. Furthermore, $\bar{f}(\phi)$ evolves monotonically between the major and minor principle directions. Truncating Eq. (3) at second order leads to an optimization problem (maximizing $\tau$) with two parameters, $\tau$ and $b_2$, bounded by demanding $\bar{f}(\phi)$ and its second derivative to be non-negative at $\phi = 3\pi/4$. The first condition reflects the purely repulsive nature of the forces, while the second ensures monotonic variation between major and minor directions. The solution to this linear program is $\tau = \tau_m = 2/3$ and $b_2 = 1/3$, so the maximum average force modulation is given by

$$\bar{f}_{\max}(\phi) = 1 + 4/3 \sin 2\phi - 1/3 \cos 4\phi. \quad (4)$$

Figures 3(b) and 3(d) illustrate the relevance of this bound for strongly hyperstatic packings: for $z = 6$ the maximal stress is close to $2/3$, while $\bar{f}(\phi)$ approaches the limiting form Eq. (4), indicated by the dashed line.

One can incorporate the effect of fabric anisotropy by introducing a modulated distribution of contact angles $\Phi(\phi) = \frac{1}{2\pi}(1 + p \sin 2\phi)$. This modulation now appears in the integral of Eq. (2) and modifies the upper bound to $\tau_m = \frac{7p+8}{8p+12}$. For realistic values of the anisotropy, typically $p < 0.3$ [5], the increase in $\tau_m$ is remarkably mild, e.g., $\tau_m \approx 0.70$ for $p = 0.3$. The more general case with frictional grains will be discussed elsewhere [26].

*High-dimensional ensemble.*—We now return to isotropic packings and address the dependence of the maximal shear stress $\tau_m$ on $z$. Close to isostaticity $\tau_m$ is significantly smaller than the bound obtained above—as can be seen by comparing Figs. 3(a) and 3(c). In fact, in the isostatic limit there are no adjustable degrees of freedom left and $\tau_m$ tends to zero. To understand the relation between $\tau_m$ and $z$, it is useful to consider the volume of the space of allowed force networks $\mathbf{F}_\tau$. As we show below, for any given contact network, the volume of $\mathbf{F}_\tau$ shrinks as the shear stress $\tau$ increases. At a certain $\tau = \tau_m$ the volume becomes zero, which marks the largest possible shear stress for which a solution to Eq. (1) exists. The general dependence of the $\tau_m$ on the $z$, based on our numerics, is depicted by the dashed curve in Fig. 1(a).

We quantify the "size" of $\mathbf{F}_\tau$ by the Euclidean distance $L$ between randomly chosen pairs of force networks, for given $z$ and $\tau$ [19,20]. While the distances between random points in a low dimensional space are broadly distributed, this distribution becomes increasingly sharply peaked for higher dimensional objects as is the case here. The average distance $L$ defined via

$$L^2(z, \tau) \equiv \langle \Sigma_{ij} (f_{ij} - f'_{ij})^2 \rangle \quad (5)$$

thus serves as an effective measure for the size of $\mathbf{F}_\tau$. Here the brackets denote an average over the random pairs of force networks $\{f_{ij}\}$ and $\{f'_{ij}\}$.

In Fig. 4 we show our main findings for the main properties of the force space with $\tau$. The size $L(\tau, z)$ can, surprisingly, be fitted by a simple relation of the form

$$(L/L_m)^2 + (\tau/\tau_m)^2 = 1, \quad (6)$$

which becomes particularly accurate for $z < 5$ [Fig. 4(a)].

The scaling relation Eq. (6) can be interpreted geometrically, keeping in mind that high-dimensional objects can be quite counterintuitive [Fig. 4(b)]. Let us consider the ensemble $\mathbf{F}$ that is obtained by applying all force balance equations and $\sigma_{xx} = \sigma_{yy} = 1/2$, but leaving $\sigma_{xy}$, and thus $\tau$, undetermined. $\mathbf{F}$ is a convex body of dimension $D = (z - z_c)N/2 - 2$ that has $zN/2$ facets; each facet corresponds to a certain contact force being zero. One can obtain $\mathbf{F}_\tau$ from an intersection of $\mathbf{F}$ with the codimension-one hyperplane given by the linear constraint $\sigma_{xy} = \tau/2$ [Eq. (1)]. Because of symmetry, the most "central" intersection is obtained for $\tau = 0$, while for larger values of $\tau$, the intersection is less centered and $\mathbf{F}_\tau$ is smaller.

Surprisingly, $L_m$ and $\tau_m$ approach simple scaling laws as shown in Figs. 4(c) and 4(d):

$$L_m \approx \sqrt{N(z - z_c)}, \quad (7)$$

$$\tau_m \approx 2\frac{z - z_c}{z}. \quad (8)$$

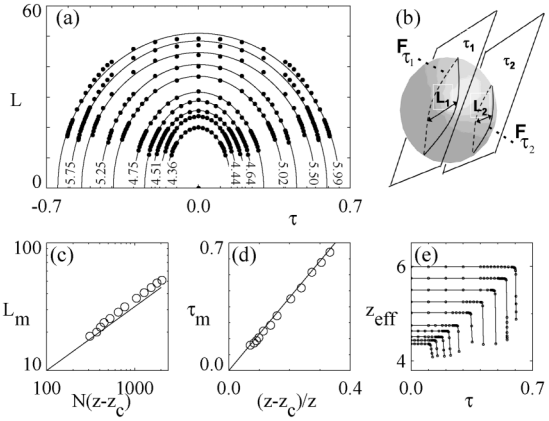


FIG. 4. (a) The linear size $L$ of the force space $\mathbf{F}_\tau$ as a function of shear stress $\tau$ for $z$ as labeled (dots) are well fitted by a relation of the form $(L/L_m)^2 + (\tau/\tau_m)^2 = 1$ (solid curves). (b) Sketch of how force space $\mathbf{F}$ (represented schematically by a sphere) intersected by the constant-$\tau$ hyperplanes yields the force spaces $\mathbf{F}_{\tau_1}$ and $\mathbf{F}_{\tau_2}$ with sizes $L_1$ and $L_2$. (c) $L_m$ obtained by fitting Eq. (6) (circles), compared to $\sqrt{N(z - z_c)}$ (line). (d) Maximal shear stress $\tau_m$ obtained by fitting Eq. (6) (circles) is well approximated by $2(z - z_c)/z$ (line). (e) $z_{\text{eff}}$ drops sharply when approaching $\tau_m$.

The scaling relation for $L_m$, Eq. (7), can be recovered analytically. The scaling $L_m \propto \sqrt{D}$ with the dimension $D = N/2(z - z_c)$ of $\mathbf{F}_\tau$ is a common feature of high-dimensional convex spaces [27]. If we consider a simple approximation for $\mathbf{F}_\tau$ by ignoring the force balance equations but only requiring that all $f_{ij}$ are positive and have $\langle f_{ij} \rangle = 1$, we directly obtain that $L^2 = 2D = N(z - z_c)$ [28]. On the other hand, for the relation for $\tau_m$, Eq. (8), we have not been able to come up with a convincing argument, but we do note that this relation implies that $\tau_m$ is proportional to the ratio between the dimension of $\mathbf{F}_\tau$, $N/2(z - z_c)$, and the number of its facets, $zN/2$.

Finally, as $\tau$ approaches its maximum $\tau_m$, the space $\mathbf{F}_\tau$ shrinks and $L \to 0$, so that at $\tau = \tau_m$, $\mathbf{F}_\tau$ consists of a single point. The effective contact number $z_{\text{eff}}$, which is defined by considering contacts broken when their force drops below a fixed small threshold [29], stays constant over most of the range of $\tau$, but sharply drops to $z_c$ as $\tau$ approaches $\tau_m$ [Fig. 4(e)].

*Outlook.*—The ensemble approach for force networks under shear provides a great conceptual simplification with respect to full numerical simulations, as it steps aside the intricate evolution of the contact network. Yet, it captures recently measured statistical properties, such as $\bar{f}(\phi)$ and the evolution of $P(f)$ [10,13]. Furthermore, it provides an alternative description of yielding phenomena, in terms of a vanishing volume of the force phase space. The precise relation between $\tau_m$ and the yield stress will have to be explored further, to see whether a system in which local rearrangements do occur before yielding can really remain jammed up to $\tau_m$. Nevertheless, in agreement with existing numerical simulations [4,7], we found that the maximum shear stress $\tau_m$ strongly depends on the coordination number of the packing. This dependence can be understood in terms of the geometry of the force space, and obeys a simple scaling law Eq. (8). The ensemble thus provides a new perspective for soil mechanics, in which relations between the macroscopic effective friction and micromechanical properties (density, coordination number, texture, etc.) play a central role. More generally, it suggests a route along which the unjamming by shear of a broad range of disordered media may be understood.

We thank L. Silbert, A. Morozov, and W. van Saarloos for discussions. J. H. S. acknowledges financial support by a Marie Curie European Fellowship FP6 (MEIF-CT2003-502006), W. G. E. from the physics foundation FOM, and T. J. H. V. and M. v. H. from the science foundation NWO through VIDI grants.

[1] A. J. Liu and S. R. Nagel, Nature (London) **396**, 21 (1998); V. Trappe *et al.*, *ibid.* **411**, 772 (2001).
[2] C. S. O'Hern, S. A. Langer, A. J. Liu, and S. R. Nagel, Phys. Rev. Lett. **86**, 111 (2001).
[3] F. Radjai, D. E. Wolf, M. Jean, and J. J. Moreau, Phys. Rev. Lett. **80**, 61 (1998).
[4] F. Radjai and S. Roux, in *The Physics of Granular Media*, edited by H. Hinrichsen and D. E. Wolf (Wiley-VCH, Berlin, 2004), pp. 165.
[5] F. Alonso-Marroquín, S. Luding, H. J. Herrmann, and I. Vardoulakis, Phys. Rev. E **71**, 051304 (2005).
[6] M. Oda, S. Nemat-Nasser, and J. Konishi, Soils Foundations **25**, 85 (1985).
[7] G. Combe and J. N. Roux, Phys. Rev. Lett. **85**, 3628 (2000).
[8] A. Kabla *et al.*, Europhys. Lett. **71**, 932 (2005).
[9] H. M. Jaeger, S. R. Nagel, and R. P. Behringer, Rev. Mod. Phys. **68**, 1259 (1996); P. G. de Gennes, *ibid.* **71**, S374 (1999).
[10] J. Geng, G. Reydellet, E. Clement, and R. P. Behringer, Physica (Amsterdam) **182D**, 274 (2003).
[11] D. M. Mueth, H. M. Jaeger, and S. R. Nagel, Phys. Rev. E **57**, 3164 (1998); D. L. Blair *et al.*, *ibid.* **63**, 041304 (2001).
[12] J. Brujic *et al.*, Faraday Discuss. **123**, 207 (2003).
[13] T. S. Majmudar and R. P. Behringer, Nature (London) **435**, 1079 (2005).
[14] E. I. Corwin, H. M. Jaeger, and S. R. Nagel, Nature (London) **435**, 1075 (2005).
[15] L. E. Silbert *et al.*, Phys. Rev. E **65**, 051307 (2002).
[16] J. P. Bouchaud, in *Slow Relaxations and Nonequilibrium Dynamics in Condensed Matter*, Proceedings of the 2002 Les Houches Summer School, Session LXXVII (EDP Sciences, Les Ulis, 2003).
[17] J. H. Snoeijer, T. J. H. Vlugt, M. van Hecke, and W. van Saarloos, Phys. Rev. Lett. **92**, 054302 (2004).
[18] J. H. Snoeijer, T. J. H. Vlugt, W. G. Ellenbroek, M. van Hecke, and J. M. J. van Leeuwen, Phys. Rev. E **70**, 061306 (2004).
[19] T. Unger, J. Kertész, and D. E. Wolf, Phys. Rev. Lett. **94**, 178001 (2005).
[20] S. McNamara and H. J. Herrmann, Phys. Rev. E **70**, 061303 (2004).
[21] B. P. Tighe *et al.*, Phys. Rev. E **72**, 031306 (2005).
[22] C. F. Moukarzel, Phys. Rev. Lett. **81**, 1634 (1998); A. V. Tkachenko and T. A. Witten, Phys. Rev. E **60**, 687 (1999).
[23] Numerical simulations [3,17] have shown that $r$ ($\approx$ grain size) does not correlate to forces and angles, so it can be taken out of the integral.
[24] For particles with $z$ contact forces, the width of the modulation is bounded from below by roughly $2\pi/z$ [4,25].
[25] H. Troadec, F. Radjai, S. Roux, and J. C. Charmet, Phys. Rev. E **66**, 041305 (2002).
[26] W. G. Ellenbroek and J. H. Snoeijer (to be published).
[27] For example, for a hypercube of dimension $D$ and edge 2 (such that the average value of any of its coordinates is one, to normalize similar to the forces), $L^2 = [D/4 \int_0^2 dx \int_0^2 dx'(x - x')^2] = 2D/3$.
[28] This space is exactly that of the microcanonical ensemble for a finite number of forces, for which $P(f) = e^{-f}$. For such a space dimension of $D$, we find that $L^2 = D \int_0^\infty dx \int_0^\infty dx'(x - x')^2 \exp(-x) \exp(-x') = 2D$.
[29] We consider a contact broken when $f < 10^{-4}\langle f \rangle$, and we have verified that results are independent of this cutoff.